NANO EXPRESS

Modification of alumina matrices through chemical etching and electroless deposition of nano-Au array for amperometric sensing

Arūnas Jagminas · Julijana Kuzmarskytė · Gintaras Valinčius · Luciana Malferrari · Albertas Malinauskas

Abstract Simple nanoporous alumina matrix modification procedure, in which the electrically highly insulating alumina barrier layer at the bottom of the pores is replaced with the conductive layer of the gold beds, was described. This modification makes possible the direct electron exchange between the underlying aluminum support and the redox species encapsulated in the alumina pores, thus, providing the generic platform for the nanoporous alumina sensors (biosensors) with the direct amperometric signal readout fabrication.

Keywords EIS · Modification morphology · Nanoparticles · Porous alumina

Introduction

Porous anodic oxide films of aluminum anodically grown in the solutions of oxalic and/or sulfuric or phosphoric acids have been used for decades as protection and hard coatings or adhesive layers. In recent years these films, so-called alumina, due to their honeycomb high-ordered and well-predetermined structure, showing tube shaped pore array with a center-to-center spacing from few tents to about 550 nm [1, 2] and the pore diameter from about 10 to 250 nm [3], are widely used as a host material for fabrication nanostructured arrays of metals, [4–6] semiconductors, [7–9] conducting polymers, [10] and carbon tubes [11, 12]. Notably, that high-ordered alumina matrices filled with nanowires or nanotubes of desired material are promising candidates for catalyst, [13] functional electrodes, [14] future sensors, [15, 16] magnetic, [17] and optoelectronic [18, 19] devices. Furthermore, high-ordered alumina membranes recently have been used for detection DNA sequences at the nmol cm^{-2} level, [20] preparation of new biochemical reactor systems, [21] and the synthesis of nano-black lipid membranes [22]. The use of anodized aluminum electrodes as support for amperometric sensors is, however, unexplored due to high resistance of alumina a thin scalloped barrier-oxide layer separated the thick porous one from the metal [23] that is a key problem. On the other hand, the development of such system within the porous alumina matrix may lead to construction of novel redox biosensor configurations. In present paper, we describe a simple nanoporous alumina matrix modification procedure, in which the electrically highly insulating barrier layer at the bottom of the pores is replaced with the gold beds. This modification makes possible the direct electron exchange between the underlying aluminum support and the redox species encapsulated in the alumina pores, thus, providing the generic platform for the nanoporous alumina sensors (biosensors) with the direct amperometric signal readout.

A. Jagminas (✉) · J. Kuzmarskytė · A. Malinauskas
Institute of Chemistry, Goštauto 9, 01108 Vilnius, Lithuania
e-mail: jagmin@ktl.mii.lt

G. Valinčius
Institute of Biochemistry, Mokslininkų 12, 08412 Vilnius, Lithuania

L. Malferrari
Instituto Nacionale di Fisica Nucleare, viale Berti-Pichat 6/2, 40127 Bologna, Italia

Experimental details

Several different aluminum sheets, which purity ranged from 98.0 to 99.99% (Goodfellow, Cambridge Ltd.), were tested as precursors for the porous anodic oxide film fabrication. The samples in the form of the flag-shape plates (7 × 7 × 0.2) mm were annealed at 500 °C for 3 h, chemically cleaned, rinsed, and electropolished before use, as usually. Porous oxide films of from 3 to 10 μm thick were grown under the anodizing cell voltage control in either an aqueous oxalic (0.3 M; 17 °C; 40 V) or phosphoric (0.04 M; 16 °C; 150 V) acid solution. To destroy the insulating barrier oxide layer only at the bottom of pores, several electrochemical and chemical etching steps were used. The alumina nanoporous layer modification included: (i) stepwise decrease of anodizing voltage (U_a) at the end of the film growth down to $U_{a,fin}$; (ii) chemical etching in a solution of 0.5 M phosphoric acid at 30 °C for time τ_w and (iii) electroless deposition of zinc/nickel layer in the immersion solution of zinc and nickel fluorborates (0.17 M $Zn(BF_4)_2$ + 0.87 M $Ni(BF_4)_2$ + 0.38 M NH_4BF_4) at room temperature for time τ_{im}. The completeness of deletion the alumina barriers at the bottom of pores was checked after each treatment step using scanning electron microscopy (SEM) (a Philips 30 L microscope equipped with energy dispersed X-ray spectrometer) and electrochemical impedance spectroscopy (EIS). The EIS measurements were carried out using a Solartron system that includes model 1286 potentiostat and model 1250 frequency response analyzer (Farnborough, UK). The EIS experiments were conducted in a frequency range of 1 Hz–100 kHz, with equal spaced data points on a logarithmic scale and with ten measurements per decade. To avoid nonlinear responses the amplitude of applied sinusoidal ac signal was set to 10 mV. The spectral data were analyzed/fitted with ZView software (Scribner Associates, South Pines, NC, USA).

Electrochemical measurements were carried out using a three-electrode polystyrene cell (2 ml) with a 6-mm-i.d. Kalrez™ O-ring, which set up the exposed to solution surface area of the working electrode to 0.32 ± 0.02 cm². A platinum coil (~4 cm²) and Ag/AgCl/KCl$_{sat}$ (Microelectrodes, Inc., Bedford, NH) were used as the auxiliary and reference electrodes, respectively. EIS measurements were carried out at 0 V bias versus the reference electrode at 20 ± 1 °C in aerated 10 mM sodium phosphate buffer (pH 7.0) solution containing 100 mM sodium sulphate.

For backside observations of the film morphology the alumina matrices were detached from substrate by dissolution of aluminum as described by Li et al. [1, 11].

Voltammetric behavior of alumina matrices was studded using a PI 50-1 potentiostat (Belarus) interfaced through a home-made analogue to a digital converter with a PC and a PR-8 programmer (Belarus). All experiments were carried out at a temperature of 20 ± 0.2 °C in a conventional three-electrode cell. The working electrode was either a vertical Au disc of 1 cm² geometric area, made from a mat polycrystalline Au sheet (99.99% purity), or alumina/nano-Au/Al of a same geometric area. A Pt sheet 3 cm² in area was a counter-electrode and a saturated potassium silver-silver chloride electrode (SCE) was used as a reference. In order to avoid the contamination of the working solution {5 mM $K_3[Fe\{CN\}_6]$ + 5 mM $K_4[Fe\{CN\}_6]$} with Cl⁻ ions, the SCE was connected to the electrochemical cell through a 1 M KCl with agar-agar jelly bridge. Prior to each experiment, the working solution was deaerated with argon.

All solutions were prepared using highest purity acids, chemically pure salts and Milli-Q water.

Reproducibility of the measurements was checked by 3 repeated experiments.

Results and discussion

We found that the quality of perforation of alumina matrices at the bottom of the pores and the ability to form there well-adhered Zn/Ni layer depend strongly on the aluminum purity as well as on the parameters of post-treatment processes, e.g. $U_{a,fin}$, τ_w, and τ_{im}. No uniform deposition of Zn/Ni layer at the bottom of pores was observed in the case of high purity aluminum electrodes (>99.9%). Instead, good quality immersion Zn layers were obtained using 99.685% purity aluminum (Si 0.156; Fe 0.089; Zn 0.03; Mg 0.021; Cu 0.016; Mn, Ti, Cr and Pb 0.003 wt.%). This is consistent with the experimental facts indicating preferable formation of Zn/Ni immersion layer on the surfaces plate of aluminum alloys [24].

Figure 1 show the cross-sectional and backside SEM images of the oxalic acid alumina matrices grown onto 99.685% purity aluminum at $U_a = 40$ V for 1.5 h after the perforation of alumina barriers by decreasing U_a down to $U_{a,fin} = 5.0$ V and subsequent etchings in the phosphoric acid and immersion solutions for 22 and 7 min, respectively. Notably, all these procedures lead to the formation of alumina matrix with diameter pores of ~ 45 nm and the interpore distance of ~ 108 nm without detachment the porous matrix from the
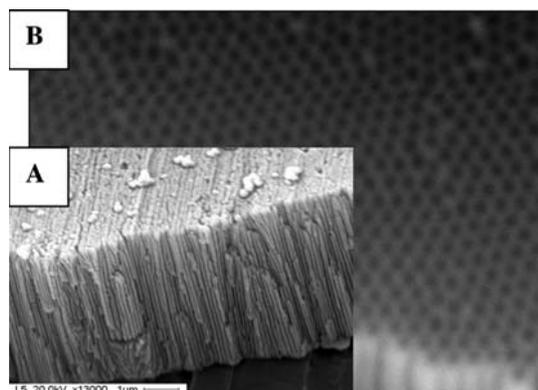
Fig. 1 The back-side (**A**) and the cross-sectional (**B**) SEM images of alumina matrices grown in a solution of 0.3 M $(COOH)_2$ at 40 V and 17 °C for 1.5 h onto the surface of 99.685 % purity Al followed by decrease of anodizing voltage down to $U_{a,fin} = 5.0$ V and subsequent etching in 0.5 M H_3PO_4 at 30 °C for $\tau_w = 22$ min

substrate. The optimal perforation conditions of the phosphoric acid films included the gradual decrease of the anodizing end-voltage from 150 V to $U_{a,fin}$ 25–27 V and the subsequent chemical etching steps for $\tau_w = 55$–65 min and $\tau_{im} = 5$–7 min resulting in the fabrication of alumina with average diameter of pores close to 200 nm and the center-to-center spacing of ~ 410 nm (Fig. 2). Notably, all these post-anodizing procedures lead not only to the perforation of the alumina nano-channels but also to the deposition of a thin Zn^0/Ni^0 immersion layer at the aluminum/solution interface at the bottom of pores. Furthermore, seeking to cover the bottoms of opened pores with well-adherent layer of precious metal, gold electroless deposition process was chosen in a 10 mM $HAuCl_4$ + 50 mM $MgSO_4$ solution by experimental way. The stored of alumina/Zn/Al electrodes in this solution leads to the formation of gold beds by the chemical exchange reaction between
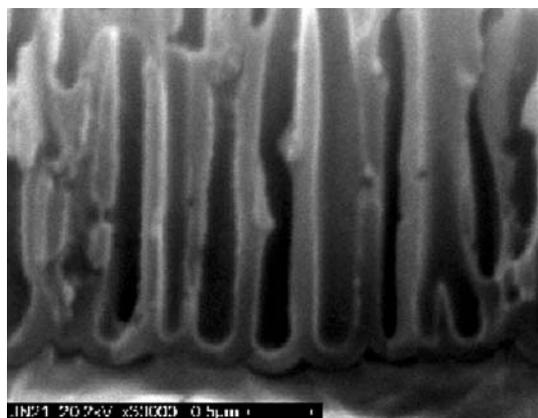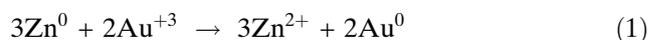

Fig. 2 The cross-sectional SEM image of alumina matrix grown in a solution of 0.04 M H_3PO_4 at 150 V and 16 °C for 2 h; $U_{a,fin} = 27.0$ V; $\tau_w = 60$ min

the Au^{3+} ions and the metallic Zn layer deposited at the places of opened pores:

$$3Zn^0 + 2Au^{+3} \; \rightarrow \; 3Zn^{2+} + 2Au^0 \tag{1}$$

As a result of this treatment, gray color of the alumina matrix acquired during zinc deposition turns into olive signaling of the formation of the nano-Au species. This was verified there by recording UV-Vis spectra of the alumina matrices detached from the substrate. The spectra in Fig. 3B show the emerging of absorbance maximum at 535–550 nm wavelength range, characteristic for gold colloids. The red-shift of the surface plasmon resonance peak seen as the immersion time increases confirms the growth of nano-Au particles [25] at the bottom part of the pores. In addition, the deposition of gold particles at the bottom of the alumina pores has been also visualized by SEM images of the matrix cross-sections (Fig. 3A) and EDX analysis data (Fig. 3C).

To characterize the electrical properties of alumina matrices, the EIS spectra were taken at each step of alumina formation and modification. Figure 4 depicts typical Bode plots of the electrode admittance of the aluminum electrode at different stages of the oxide matrix formation and re-construction. A systematic variation of the EIS spectra in Fig. 4 includes the increase of electrode admittance in the low frequency range and the shift of admittance curves towards lower frequencies. The shift of the admittance plots indicates the capacitance increase upon the successive steps of alumina matrix post-treatment, which, as we believe, considerably decreases or even fully removes the insulating barrier. The capacitance increase is clearly seen in the complex capacitance curves as well as in the fitting to model [26, 27] parameters, which are presented in the Supporting Information section. The most important result that follows from Fig. 4 is a noticeable increase of the admittance in the low frequency edge of the spectra. Particularly, the formation of the immersion zinc layer at the bottom of the pores yields approximately 3 fold increase, while the gold beds formed in following stage increases the admittance by approximately 25–30 times compared to the initial admittance values of the chemically unmodified alumina. Moreover, the EIS spectra of pure alumina (Fig. 4, curve 1) were not significantly altered by the addition of the redox species to the electrolyte, while the gold-modified alumina matrices exhibited clear sensitivity to the potassium ferrocyanide (curve 4). The redox species especially influenced the low frequency part of the EIS spectra, in which the weight of the Faradaic processes contribution to the EIS signal
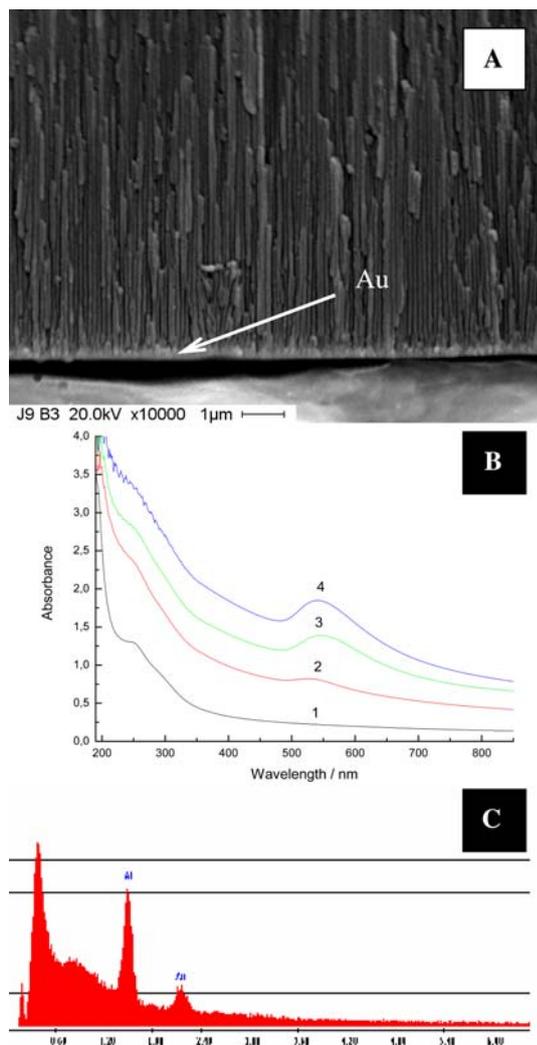
Fig. 3 (**A**) Cross-sectional SEM image of alumina matrix grown as in Fig. 1 after the additional treatment in the Zn/Ni immersion solution (pH 6.0) at RT for 5 min and electroless gold plating at RT for 5 min. (**B**) UV-vis spectra of alumina matrices fabricated as in (**A**) on the gold plating time: (1) 0; (2) 2; (3) 5; (4) 15 min. (**C**) EDX spectra of alumina matrix grown and re-constructed as in part *B* (curve 3)

becomes significant. In our case, the electrode admittance at 1 Hz increased from ~50 to 150 μS (electrode surface–0.32 cm^2) upon injection of potassium ferrocyanide at concentration of 10 mM (compare curves 3 and 4). All this suggests that the alumina modification procedures used in this work yield nanoporous electrodes, on which the direct electron exchange between the dissolved redox species and the underlying metal becomes possible.

To probe the direct electron transfer rate we compared the cyclic voltammetry response of the metal gold and gold-modified alumina electrodes using ferri/ferro cyanide redox system under the same experimental conditions. Figures 5A and B illustrate typical
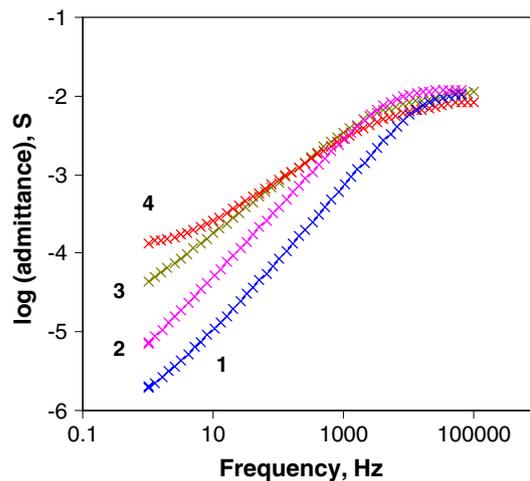

Fig. 4 Bode plots of admittance of Al/alumina electrodes within 1–100,000 Hz frequency range corresponding to different stages of the barrier layer deletion: (1) after anodization of Al specimen in 0.04 M H$_3$PO$_4$ (U_a 150 V; 3.0 h; 16 °C followed by step-like voltage decrease to $U_{a,fin}$ 27.0 V and chemical pore widening for τ_w 60 min); (2) after formation of Zn^0 layer at the bottom of the pores by immersion in a solution of Zn/Ni fluorborates for 7 min; (3) after replacement of zinc by gold via chemical exchange reaction; (4) the same as (3), however, the pore-filling solution contains additionally the redox species [10 mM K$_4$Fe(CN)$_6$] (vide infra). Electrode surface area exposed to the solution is 0.32 cm^2. Temperature 20 °C

cyclic voltammograms (CVs) obtained in a solution of 10 mM K$_3$[Fe(CN)$_6$]/K$_4$[Fe(CN)$_6$] (1:1) using polycrystalline Au plate (99,9% purity) and gold-modified alumina electrodes. As seen, the shapes of CVs are comparable both qualitatively and quantitatively. In particular, potential difference between cathodic and anodic peaks ΔE_p, equals ~200 mV at potential scan rate of 50 mV/s. Similar current-potential behavior of the bulk and nanostructured gold electrodes imply that the rate of electron transfer reactions taking place at both electrodes are similar. This is an important result because it suggests that the modification route of the nanoporous alumina surfaces presented in this work makes available full removal of the alumina barrier layer from the bottom of the pores.

Conclusions

Complete deletion of the alumina barrier layer only at the bottom of the pores can be attained through step-wise decrease of anodizing voltage, several steps of chemical etching and electroless deposition of nano-Au species at the bottom of alumina pores at the aluminum/solution interface. By this way, the low resistant nano-Au/alumina/Al electrode for amperometric sensing was fabricated.
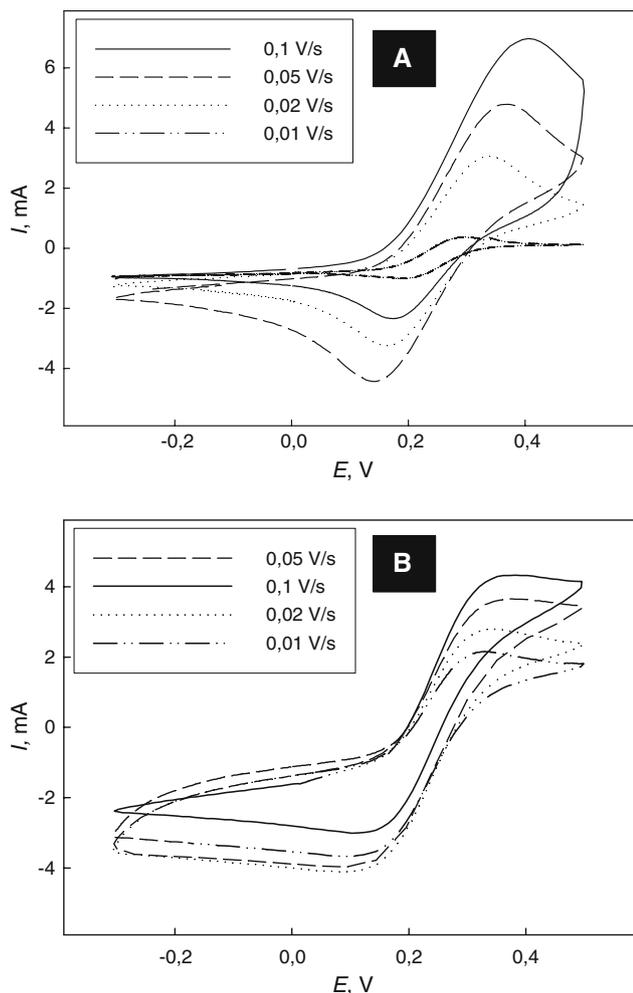
Fig. 5 Cyclic voltammograms of the gold plate (**A**) and nano-Au/alumina/Al (**B**) electrodes fabricated as in Fig. 1 in a deaerated and unstirred 10 mM $K_3[Fe(CN)_6]/K_4[Fe(CN)_6]$ (1:1) buffered solution (acetate buffer; pH = 6.0) on the potential scan rate. The apparent surface area of electrodes 0.5 cm^2

Notably, the fractal structure of re-constructed alumina matrices results in the specific EIS response that can be modeled by two parallel CPEs one of which exhibits $\alpha \approx 1$ and an another $\alpha \approx 0.5$.

References

1. A.P. Li, F. Müller, A. Birner, K. Nielsch, U. Göselle, J. Appl. Phys. **84**, 6023 (1998)
2. A. Jagminas, D. Bigeliene, I. Mikulskas, R. Tomašiūnas, J. Cryst. Growth **233**, 591 (2001)
3. W. Lee, J.-K. Lee, Adv. Mater. **14**, 1187 (2002)
4. C.R. Martin, R. Parthasarathy, V. Menon, Electrochim. Acta. **39**, 1309 (1994)
5. D. Al-Mawlawi, C.Z. Liu, M. Moskovits, J. Mater. Resp. **9**, 1014 (1994)
6. C.J. Murphy, N.R. Jana, Adv. Mater. **14**, 80 (2002)
7. J.D. Klein, R.D. Herrick, I.D. Palmer, M.J. Sailor, C.J. Brumlik, C.R. Martin, Chem. Mater. **5**, 902 (1993)
8. D. Xu, Y. Xu, D. Chen, G. Guo, L. Gui, Y. Tang, Adv. Mater. **12**, 520 (2000)
9. M.S. Sander, A.L. Prieto, R. Gronsky, T. Sands, A.M. Stacy, Adv. Mater. **19**(9), 665 (2002)
10. J. Joo, K.T. Park, B.H. Kim, M.S. Kim, S.Y. Lee, C.K. Jeong, J.K. Lee, D.H. Park, W.K. Yi, G.H. Lee, K.S. Ryn, Synthetic Metals **7–9,** 135 (2003)
11. P. Li, C. Papadopoulos, J.M. Xu, M. Moskovits, Appl. Phys. Lett. **75**, 367 (1999)
12. T. Kyotani, L. Tsai, A. Tomita, Chem. Mater. **8**, 2109 (1996)
13. Y. Ishikawa, Y. Matsumoto, Electrochim. Acta. **46**, 2819 (2001)
14. A. Mozalev, S. Magaino, H. Imai, Electrochim. Acta. **46**, 2825 (2001)
15. W.G. Yelton, K.B. Pfeifer, A.W. Staton, J. Electrochem. Soc. **149**(1), H1 (2002)
16. A. Yu, Z. Liang, J. Cho, F. Caruso, Nano Lett. **3**, 1203 (2003)
17. D. Al-Mawlawi, N. Coombs, M.J. Moskovits, Appl. Phys. **70**, 4421 (1991)
18. C.K. Preston, M. Moskovits, J. Phys. Chem. **97**, 8495 (1993)
19. I. Mikulskas, S. Juodkazis, A. Jagminas, Š. Meškinis, J.G. Dumas, J. Vaitkus, R. Tomašiūnas, Optic. Mater. **17**, 343 (2001)
20. S. Pan, L.J. Rothberg, Nano Lett. **3**(6), 811 (2003)
21. Z. Wang, R.T. Haasch, G.U. Lee, Langmuir **21**(4), 1153 (2005)
22. W. Römer, C. Steinem, Biophys. J. **86**, 955 (2004)
23. J.W. Diggle, T.C. Downie, C.W. Goulding, Chem. Rev. **69**, 365 (1969)
24. G. Qi, X. Chen, Z. Shao, Thin Solid Films. **406**, 204 (2002)
25. S. Link, M.A. El-Sayed, J. Phys. Chem. **B 43**, 4519 (2004)
26. A. Jagminiene, G. Valinčius, A. Riaukaite, A. Jagminas, J. Cryst. Growth **274**, 622 (2005)
27. J. De Laet, H. Terryn, J. Vereecken, Electrochim. Acta. **41**, 1155 (1995)